CDF/PHYS/TOP/GROUP/9048
Version 0.2
17th December 2007

Top Quark Mass Measurement in the 2.1 fb^{-1} Tight Lepton and Isolated Track Sample using Neutrino ϕ Weighting Method

Igor Suslov[1], Marco Trovato[2], Vladimir Glagolev[1], George Velev[3], Oleg Pukhov[1], Giorgio Bellettini[2], Julian Budagov[1], Guram Chlachidze[1,3], Alexei Sissakian[1]

Abstract

We report on a measurement of the top quark mass in the Tight Lepton and Isolated Track Sample using the Neutrino ϕ Weighting Method. 236 events were obtained after applying the selection cuts for the data sample with the integrated luminosity of 2.1 fb^{-1}. These events were reconstructed according to the $t\bar{t}$ hypothesis and fitted as a superposition of signal and combined background. For the expected number of background 105.8±12.9 we measure the top quark mass to be $M_{top} = 167.7 \pm^{4.2}_{4.0}$ (stat) ± 3.1 (syst) GeV/c^2.

[1]JINR, Dubna

[2]INFN and Department of Physics, University of Pisa

[3]Fermilab

Contents

1 Introduction 3

2 Principles of the Method 3
- 2.1 Constrained variables . . . 3
- 2.2 Fitter procedure . . . 4
  - 2.2.1 The χ^2 form . . . 4
  - 2.2.2 Scanning of the (ϕ_1, ϕ_2) plane . . . 5
  - 2.2.3 Weighting the solutions . . . 7
- 2.3 Picking up the solution . . . 9
- 2.4 Likelihood Form . . . 9

3 PHI Method optimization 10

4 Event Selection 14

5 Templates 15
- 5.1 Monte Carlo Signal Templates . . . 15
- 5.2 Background template . . . 17

6 Results from pseudo-experiments 19

7 Blind test results 23

8 Systematic Uncertainties 25
- 8.1 Jet Energy Scale . . . 25
- 8.2 Radiation effects, generators and B-jet energy scale . . . 25
- 8.3 Background Shape . . . 27
- 8.4 Parton Distribution Functions . . . 29
- 8.5 Lepton energy scale . . . 30
- 8.6 Summary of Systematic Errors . . . 31

9 Data 31

10 Conclusion 34

Bibliography 42

1 Introduction

In this note, we present a top mass measurement in the *dilepton* channel using the Neutrino ϕ Weighting Algorithm (PHI). This method was successful applied twice to the CDF II data: at the statistics 190 pb^{-1} [1] and later on at the statistics 340 pb^{-1} [2]. The last result was published at PRD[3].

Brief description of this method is in this note below. Some changes in χ^2 compare to the previous analysis were applied as further method development. In order to increase the statistical resolution we modified the χ^2 including the dependence t-quark width vs. M_t. Also the transfer functions were applied for more accurate description of b-parton responses.

The integrated luminosity of the data sample is 2.1 fb^{-1}. b-tag information was not used in this analysis. Monte Carlo (MC) samples were produced by 6-th generation of the CDF simulation and reconstruction programs.

For this analysis we applied the lepton + track event selection to collect more events due to the relaxed cuts for one of the leptons.

2 Principles of the Method

2.1 Constrained variables

We have unconstrained kinematic situation for the "PHI" method: a total number of 24 unknown (b, $\bar{b}$, l^-, l^+, ν, $\overline{\nu}$ 4-momenta) and only 23 equations (measured 3-momenta for two b-jets and two leptons, assumed knowing mass for 6 final particles, used two transverse components of calorimeter missing energy, constrained invariant mass for two W and assumed equal constrained mass of top and antitop quarks) to constrain the kinematics.

Obviously, it is impossible to pick up directly only one solution per event. We must assume some of the event parameters ($\vec{R}$); as known, in order to constrain the

kinematics and then vary the $\vec{R}$ to determine the variety of solutions. In addition, every solution must have a weight attached to it.

The minimal requirement in the case of $-1C$ kinematics to perform the χ^2 minimization is to use a two dimensional vector as $\vec{R}$. For our analysis we choose the azimuthal angles of the neutrino momenta $\vec{R} = (\phi_{\nu 1}, \phi_{\nu 2})$ and create a net of solutions in the $(\phi_{\nu 1}, \phi_{\nu 2})$ plane.

2.2 Fitter procedure

In this section we will clarify the idea about the tool, called "Fitter". The "Fitter" receives as input a set of information about a selected event and gives at output array of the reconstructed top quark masses with appropriate weights per event.

2.2.1 The χ^2 form

The **Fitter** uses final particles momentum, jet energy information as well as constraints on W and t masses. The common formula for χ^2 is:

$$\chi^2 \equiv -2ln(\mathscr{P}(\mathbf{x})) \tag{1}$$

where $\mathbf{x}$ is a general notation to indicate a variable and $\mathscr{P}$ its probability density distribution.

The expanded formula of χ^2 is :

$$\begin{aligned}
\chi^2 &= \chi^2_{reso} + \chi^2_{constr} \qquad (2)\\
\chi^2_{reso} &= \sum_{l=1}^{2} \frac{(P_T^l - \tilde{P}_T^l)^2}{\sigma_{P_T^l}^2} + \sum_{j=1}^{2}[-2ln(\mathscr{P}_{tf}(\tilde{P}_T^j|P_T^j))] + \sum_{i=x,y} \frac{(UE^i - \tilde{UE}^i)^2}{\sigma_{UE^i}^2}\\
\chi^2_{constr} &= -2ln(\mathscr{P}_{BW}(m_{inv}^{l_1,\nu_1}|M_W,\ \Gamma_{M_W})) - 2ln(\mathscr{P}_{BW}(m_{inv}^{l_2,\nu_2}|M_W,\ \Gamma_{M_W})) +\\
&\quad -2ln(\mathscr{P}_{BW}(m_{inv}^{l_1,\nu_1,j_1}|\tilde{M}_t,\ \Gamma_{\tilde{M}_t}) - 2ln(\mathscr{P}_{BW}(m_{inv}^{l_2,\nu_2,j_2}|\tilde{M}_t,\ \Gamma_{\tilde{M}_t}))
\end{aligned}$$

The variables with a tilde sign refer to the output of the minimization procedure, whereas P_T and UE (unclustered energy) represent measured values corrected for known detector and physics effects. $\tilde{M}_t$ is the fit parameter giving the reconstructed top mass. BW and tf are for the relativistic Breit-Wigner and transfer function respectively.

Notice that we splitted the χ^2 into two parts: the first one, χ^2_{reso}, takes into account the detector uncertainties, whereas the second one deals with the known mass constraints.

The first sum (in χ^2_{reso}) runs over the primary lepton (tight lepton) and the track lepton. We take the uncertainties for the lepton and track lepton from the Run I studies [4]:

$$\frac{\sigma^e_{P_T}}{P^e_T} = \sqrt{\frac{a}{P^e_T} + b} \tag{3}$$

$$\frac{\sigma^\mu_{P_T}}{P^\mu_T} = c \cdot P^\mu_T \tag{4}$$

where $a = 0.135^2$, $b = 0.02^2$, $c = 0.0011$.

The second sum (in χ^2_{reso}) is over the two leading jets. These transverse momenta have been further corrected for multiple interactions, underlying event and out-of-cone energy (level 6 and 7), even though only level-5 corrected jets were considered for selection purposes.

The third sum (in χ^2_{reso}) is over the two transverse components of the unclustered energy[1].

The other term in the formula (2), χ^2_{constr}, refers to the invariant masses of the couples lepton-neutrino and of the lepton-neutrino-leading jet system. We set $M_W = 80.41 GeV/c^2$, $\Gamma_{M_W} = 2.06 GeV/c^2$, and we insert the function Γ_{M_t} (see Figure 1), according to the standard model [5].

The insertion of the top width dependence from the top mass is new for our analysis. We will discuss obtained improvement later in this note.

2.2.2 Scanning of the $(\phi_1,\ \phi_2)$ plane

We should find the solutions over the (ϕ_1, ϕ_2) variety: we optimized the step [3] and we scan all the $(0, 2\pi) \times (0, 2\pi)$ (ϕ_1, ϕ_2) net. The net is chosen to have 12x12 points for $(0, \pi) \times (0, \pi)$ (ϕ_1, ϕ_2). For each point of the net we can write the following linear system:

$$\begin{cases} P_T^{\nu_1} cos(\phi_{\nu_1}) + P_T^{\nu_2} cos(\phi_{\nu_2}) = \not\!\!E_{T_x} \\ P_T^{\nu_1} sin(\phi_{\nu_1}) + P_T^{\nu_2} sin(\phi_{\nu_2}) = \not\!\!E_{T_y} \end{cases} \tag{5}$$

[1] UE is defined as the sum of all unclustered energy in the calorimeter, that is the sum of all the towers which are not associated with any of the objects previously considered in the χ^2 formula (tight lepton, track lepton, two leading jets): notice that this definition also includes remaining jets with $E_T > 8\ GeV$ and $|Eta| < 2$ which are not already taken into account as leading jets.

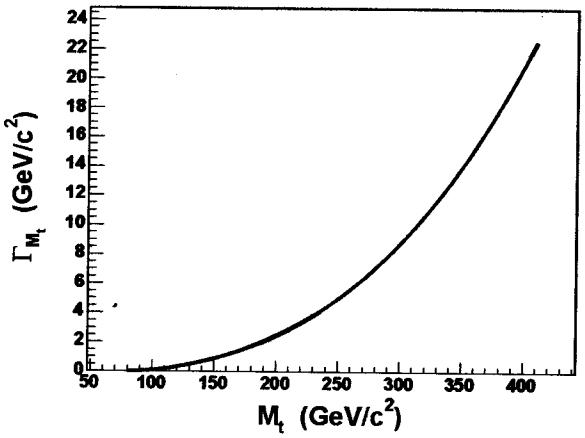

Figure 1: Top width vs. top mass

which is solved by:

$$\begin{cases} P_x^{\nu 1} \equiv P_T^{\nu 1} \cdot cos(\phi_{\nu 1}) = \frac{\not{E}_{T_x} \cdot sin(\phi_{\nu 2}) - \not{E}_{T_y} \cdot cos(\phi_{\nu 2})}{sin(\phi_{\nu 2} - \phi_{\nu 1})} \cdot cos(\phi_{\nu 1}) \\ P_y^{\nu 1} \equiv P_T^{\nu 1} \cdot sin(\phi_{\nu 1}) = \frac{\not{E}_{T_x} \cdot sin(\phi_{\nu 2}) - \not{E}_{T_y} \cdot cos(\phi_{\nu 2})}{sin(\phi_{\nu 2} - \phi_{\nu 1})} \cdot sin(\phi_{\nu 1}) \\ P_x^{\nu 2} \equiv P_T^{\nu 2} \cdot cos(\phi_{\nu 2}) = \frac{\not{E}_{T_x} \cdot sin(\phi_{\nu 1}) - \not{E}_{T_y} \cdot cos(\phi_{\nu 1})}{sin(\phi_{\nu 1} - \phi_{\nu 2})} \cdot cos(\phi_{\nu 2}) \\ P_y^{\nu 2} \equiv P_T^{\nu 2} \cdot sin(\phi_{\nu 2}) = \frac{\not{E}_{T_x} \cdot sin(\phi_{\nu 1}) - \not{E}_{T_y} \cdot cos(\phi_{\nu 1})}{sin(\phi_{\nu 1} - \phi_{\nu 2})} \cdot sin(\phi_{\nu 2}) \end{cases} \quad (6)$$

Since we add two additional values, we perform a *1C* fit minimization of the χ^2 (2). This is done for every point of the net, with a particular attention to avoid those ones satisfying the equation $\phi_{\nu_1} - \phi_{\nu_1} = k \cdot \pi$ with $k = 0, 1$ (in practice there is no limitation because we optimize the net by avoiding these points).

We must notice that we would have the same components of the neutrino's momentum $P_{x,y}^{\nu_1,\ \nu_2}$ for $\phi'_{\nu 1,\nu 2} = \phi_{\nu 1,\nu 2} + \pi$ (see 6) and we would take into accounts three unphysical solutions ($P_T^{\nu 1} < 0$ and/or $P_T^{\nu 2} < 0$). We subdivide the whole net we should scan $(0, 2\pi) \times (0, 2\pi)$ into 4 areas: $(0, \pi) \times (0, \pi)$, $(0, \pi) \times (\pi, 2\pi)$, $(\pi, 2\pi) \times (0, \pi)$, $(\pi, 2\pi) \times (\pi, 2\pi)$.

We stay away from the unphysical solutions by scanning a $(0, \pi)(0, \pi)$ net and

by changing sign to $P_T^{\nu 1(\nu 2)}$ in the case we find the negative neutrino momentum. This automatically change the phi quadrant as shown by the equation below:

$$\phi'_{\nu 1(\nu 2)} = \phi_{\nu 1(\nu 2)} + \pi \implies P'_{x,y}{}^{\nu 1(\nu 2)} = P_{x,y}^{\nu 1(\nu 2)} \text{ and } P_T'^{\nu 1(\nu 2)} = -P_T^{\nu 1(\nu 2)}$$

Starting from the 8 solutions per net point per event (longitudinal momentum component for every neutrino has two solutions and there is an ambiguity in coupling W with b-jets) we can finally say that we have to do 1152 $1C$ minimizations which return the $\widetilde{M}_{t_{ijk}}$ and χ^2_{ijk} ($i = 1, \ldots, 12$; $j = 1, \ldots, 12$; $k = 1, \ldots, 8$) at the output.

2.2.3 Weighting the solutions

In section 2.2.1 we apply the Breit-Wigner functions inside the χ^2 formula (2) for W and t invariant mass distributions. The relativistic Breit-Wigner formula is:

$$BW(m_{inv}|\, m, \Gamma) \sim \frac{1}{(m_{inv}^2 - m^2)^2 + m^2\Gamma^2} \tag{7}$$

For our analysis we decided to use the next Breit-Wigner normalization to obtain the top mass solutions:

$$BW(m_{inv}|\, m, \Gamma) = \frac{\Gamma^2 \cdot m^2}{(m_{inv}^2 - m^2)^2 + m^2\Gamma^2} \tag{8}$$

where m and Γ are the mass and the decay width for t or W particles, depending on the considered decay chain; m_{inv} refers to the invariant mass, calculated with the appropriate information from lepton and neutrino, in case of W decay, or lepton, neutrino and leading jet, in case of t decay.

In case of $W \to l\nu$ Breit-Wigner, formula (8) has a constant decay width, which has not any importance in the χ^2 minimization. Instead of Γ_t depends of the χ^2 minimization parameter (top mass, see Figure 1).

Our investigation shows that the distribution of reconstructed masses has the smaller error and the more accurate mean value if we apply for the solutions weights renormalized Breit-Wigner formula:

$$BW(m_{inv}|\, m, \Gamma) = \frac{\Gamma \cdot m^2}{(m_{inv}^2 - m^2)^2 + m^2\Gamma^2} \tag{9}$$

This function is normalized to 1, instead of the previous one which has the maximum independent of the top mass: see Figure 2. We select the lowest χ^2 solution

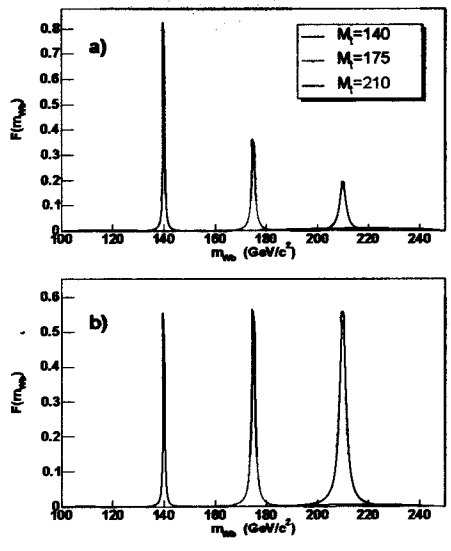

Figure 2: The relativistic Breit-Wigner functions: top - equation (9), bottom - equation (8)

out of 8 with associated mass for every point of the (ϕ_1, ϕ_2) net, this way we reduce the number of obtained masses to 144 per event. Each of these masses should be taken into account because each of them arise from a particular and physical configuration of our event.

Then we are using the χ^2 definition (according to (9)) to give a probability of occurence for our 144 solutions. The expression for the weight is given below:

$$w_{ij} = \frac{e^{-\frac{\chi^2_{ij}}{2}}}{\sum_{i,j=1}^{12} e^{-\frac{\chi^2_{ij}}{2}}}; \qquad i,j = 1,\ldots,12 \tag{10}$$

this formula is obtained by inverting (1) and normalized by 1.

2.3 Picking up the solution

Once we have found the weight for each of the 144 masses per event, we define an optimized procedure to obtain the final reconstructed mass per event. The procedure follows the steps below:

1. We build a mass probability density distribution (PDD) by using w_{ij} and $\widetilde{M_{t_{ij}}}$ info: we have 144 entries per event.
2. We identify the most probable value (MPV).
3. We calculate M_t^{reco} by averaging the PDD bins with values above treshold=0.3 from MPV which was optimized and described in the CDF internal note [2].

2.4 Likelihood Form

The likelihood function finds the probability that our data candidates are described by an appropriate admixture of background events and dilepton $t\bar{t}$ decays with a certain top quark mass.

We perform comparison by parametrizing the mass distributions in Monte Carlo templates, reconstructing an M_t^{reco} on the data sample and finally matching the two by using the likelihood unbinned fit and minimization.

The likelihood function has the following form:

$$\mathscr{L} = \mathscr{L}_{shape} \cdot \mathscr{L}_{backgr} \cdot \mathscr{L}_{param}; \tag{11}$$

where

$$\mathscr{L}_{shape} = \frac{e^{-(n_s+n_b)} \cdot (n_s+n_b)^N}{N!} \cdot \prod_{n=1}^{N} \frac{n_s \cdot f_s(m_n|M_{top}) + n_b \cdot f_b(m_n)}{n_s+n_b} \tag{12}$$

and

$$\mathscr{L}_{backgr} = exp(\frac{-(n_b - n_b^{exp})^2}{2\sigma_{n_b}^2}) \tag{13}$$

$$\mathscr{L}_{param} = exp\{-0.5[(\vec{\alpha}-\vec{\alpha_0})^T U^{-1}(\vec{\alpha}-\vec{\alpha_0}) + (\vec{\beta}-\vec{\beta_0})^T V^{-1}(\vec{\beta}-\vec{\beta_0})]\}. \tag{14}$$

Here U and V are the covariance matrices for the parameters $\vec{\alpha_0}$ and $\vec{\beta_0}$ respectively (see the formulaes 15 - 18).

The likelihood maximization procedure (we usually minimize $-ln(\mathscr{L})$) returns a **true top quark mass estimator** M_{top} and an estimated number of signal (n_s) and background (n_b).

We assign a probability (f_s) that each of the selected event looks like signal and the probability (f_b) that this event can be considered as background one. These two probabilities are weighted according to appropriate signal and background numbers n_s and n_b.

Moreover we want to point out that "PHI" method uncertainties in the signal and background parametrization are included directly into the statistical error estimation procedure.

3 PHI Method optimization

In this section we explain what are the improvements were obtained by upgrading the χ^2 in the formula (2) and the appropriate weights (see 10).

Basically we introduced two changes in the definition of the χ^2: 1) we switched from the approximate gaussian functions for the invariant mass constraint [2] to the more physical correct Breit-Wigner distributions, concerning to t, $\bar{t}$, $W^{\pm}$ decays, and 2) we use the m_t dependendent Γ_t instead of the constant value used before [2].

We have compared the top mass spectra reconstructed by means of the slightly different functions for the Breit-Wigner (9) and (8) included in χ^2.

In Figure 3 the plots were built by using Monte Carlo information at parton level. Only one solution per event was picked up because we do not have any ambiguities about P_z^{ν}, (ϕ_1, ϕ_2) and lepton-jets pairings. Because of this reason this check is weight-indepent. Monte Carlo generated events with $M_t = 161, 171$ and 181 GeV/c^2 were used.

The comparison shows the advantage of the function (8) applied for χ^2 minimization. As a next step of optimization we tried a different kind of weight applied to the top mass solutions.

We compared the different ways of reconstructing top invariant masses (see Figure 4):

- *Case 0*: Gaussian distribution function for both χ^2 and weight ([2]).
- *Case A*: Breit-Wigner's as in (8) for the χ^2 and for the weight
- *Case B*: Breit-Wigner's as in (9) for the χ^2 and for the weight

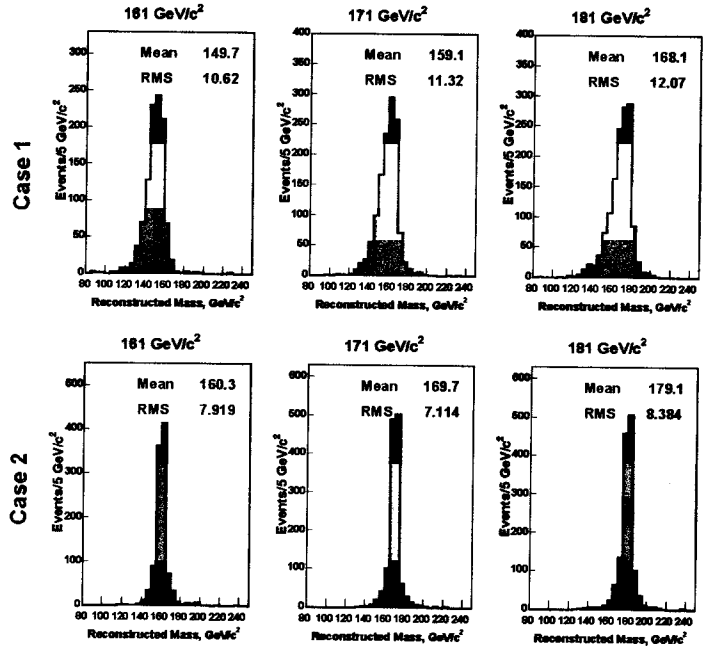

Figure 3: Top mass reconstruction at HEPG level by using Breit-Wigner (9) - top plots; and (8) - bottom plots

- *Case C*: Mixed combination: Breit-Wigner's as in (8) for the χ^2 and the weight recalculated according to Breit-Wigner function (9).

In the Figure 4 we plotted the estimated statistical errors[2] calculated by using Monte Carlo generated $t\bar{t}$ events with expected number of signal events $n_s = 60.53$ [7], versus input top quark mass.

The conclusion is clear: **The method C** is chosen as our final way since it has the best resolution. The resolution gain is about 20% compare to our previous method (Case 0).

Moreover we changed the leading jet term inside the equation (2). We switched from the formula $\sum_{j=1}^{2} \frac{(P_T^j - \widetilde{P_T^j})^2}{\sigma^j_{P_T}}$ (j runs over the two leading jets) to one that

[2]This error is obtained by performing the pseudo-experiments technique

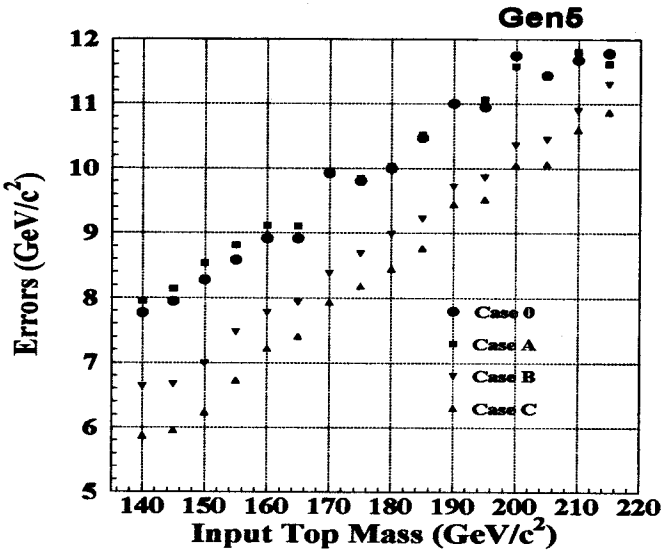

Figure 4: Improvements in final statistical errors by using M_t dependent Breit-Wigner functions and two different weights for the top mass solutions

exploits our transfer function[3].

Figure 5 represents the variable $k = (P_T^{part} - P_T^{jet})/P_T^{jet}$, fitted in different $(|\eta|, P_T^{jet})$ regions.

We used for production of these plots Monte Carlo $t\bar{t}$ events with top mass 175, 175 ± 0.5 GeV/c^2. We take into account b parton P_T dependence from M_t by adding an appropriate weight.
We do not see a big gain in respect to the previous analysis [2], as shown in Figure ??: blue dots refer to the procedure of top mass calculation performed by using transfer functions and red ones are for the old type χ^2 i.e. without this transfer functions.

[3]also called "top specific corrections"

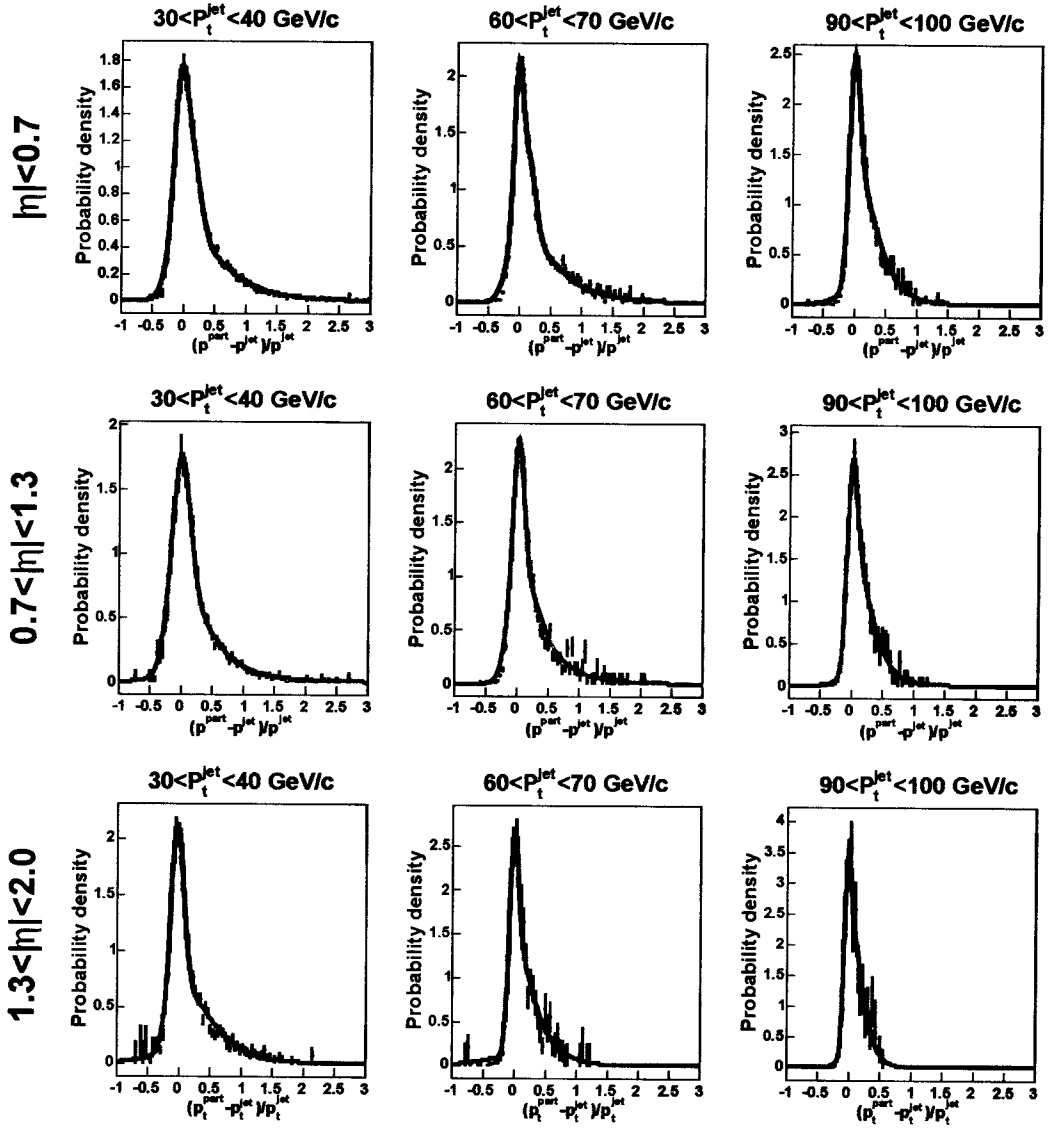

Figure 5: Top Specific Corrections

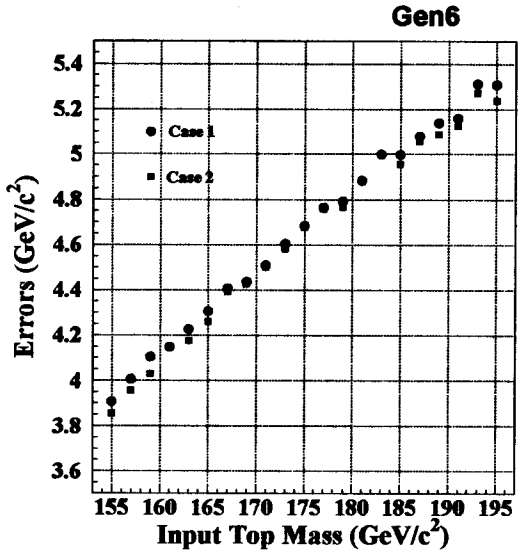

Figure 6: Stastical error improvement by using top specific corrections

4 Event Selection

In our analysis we used data collected between March 2002 and May 2007, corresponding to a total integrated luminosity of 2.1 fb^{-1}. The data are collected with an inclusive lepton trigger that requires an electron with $E_T > 18$ *GeV* or a muon with $P_T > 18$ *GeV/c*. After full event recontruction we select events with a tight electron $E_T > 20$ *GeV* or muon with $P_T > 20$ *GeV/c*, an isolated high-p_t track $P_T > 20$ *GeV/c* ("track lepton" or"tl"), two or more jets $E_T > 20$ *GeV*, and significant $\not\!\!E_T > 25$ *GeV*.

Tight electron candidates have a well-measured track pointing at an energy deposition in the calorimeter. In addition, the candidate's electromagnetic shower profile must be consistent with that expected for electrons. Tight muon candidates must have a well-measured track linked to hits in the muon chambers and energy deposition in the calorimeters consistent with that expected for muons. Tight lepton have to be isolated that means the total transverse energy within cone $\Delta R \equiv \sqrt{(\Delta\eta)^2 + (\Delta\phi)^2} < 0.4$, minus the candidate lepton E_T, is less than 10% of the candidate lepton E_T.

To count as the second lepton (track lepton) for the our analysis a well-measured track must have $P_T > 20$ GeV/c, and pass a track isolation requirement. The track isolation is defined as the ratio of the transverse momentum of the candidate track to the sum of the transverse momenta of all tracks in a cone of $\Delta R \equiv \sqrt{(\Delta\eta)^2 + (\Delta\phi)^2} < 0.4$ around it, including the candidate track itself. The track isolation value should be > 0.9.

The tight lepton and the track lepton have to be oppositely charged.

Two (or more) jets with corrected $E_T > 20$ GeV and $|\eta| < 2.0$ are also required.

If $\not\!\!E < 50$ GeV we additionally require that the angle between $\vec{\not\!\!E}$ and the nearest jet is $\Delta\phi > 25^o$.

Events with cosmic ray, conversion or Z are eliminated.

The further details of the event selection are described on the Tight Lepton and Isolated Track sample cross-section measurement [7].

After these selection cuts 236 events were left, which were reconstructed according to the $t\bar{t}$ hypothesis. The same cuts were applied to the Monte Carlo generated signal or background events.

For data from periods 8,9,10,11 we used Good Run List v17. This list was modified according to recommendations DQM group concerning to runs with unconsistent beamlines [8]. Selection over data from period 12 was performed with Good Run List v18.

5 Templates

5.1 Monte Carlo Signal Templates

The official MC samples were used. The signal templates for input top masses in the 155÷195 GeV range were created with 2 GeV steps (see the examples in Fig. 7).

Then the obtained set of templates was parametrized by one Landau and two Gaussian functions

$$f_s(M_t^{reco}|M_{top}) = p_7\left(p_6\frac{1}{\sqrt{2\pi}p_2}e^{-0.5\left(\frac{M_t^{reco}-p_1}{p_2}+e^{-\frac{M_t^{reco}-p_1}{p_2}}\right)}+\right. \quad (15)$$
$$\left.+\,(1-p_6)\frac{1}{\sqrt{2\pi}p_5}e^{-0.5\left(\frac{M_t^{reco}-p_4}{p_5}\right)^2}\right)+(1-p_7)\frac{1}{\sqrt{2\pi}p_3}e^{-0.5\left(\frac{M_t^{reco}-p_8}{p_3}\right)^2}$$

Notice that this parametrizing function is strongly dependent from the the input top mass M_{top}, or it is better to say that its parameters $p_1, \ldots, p_8$, are M_{top}-dependent:

$$p_k = \alpha_k + \alpha_{k+8} \cdot M_{top} \tag{16}$$

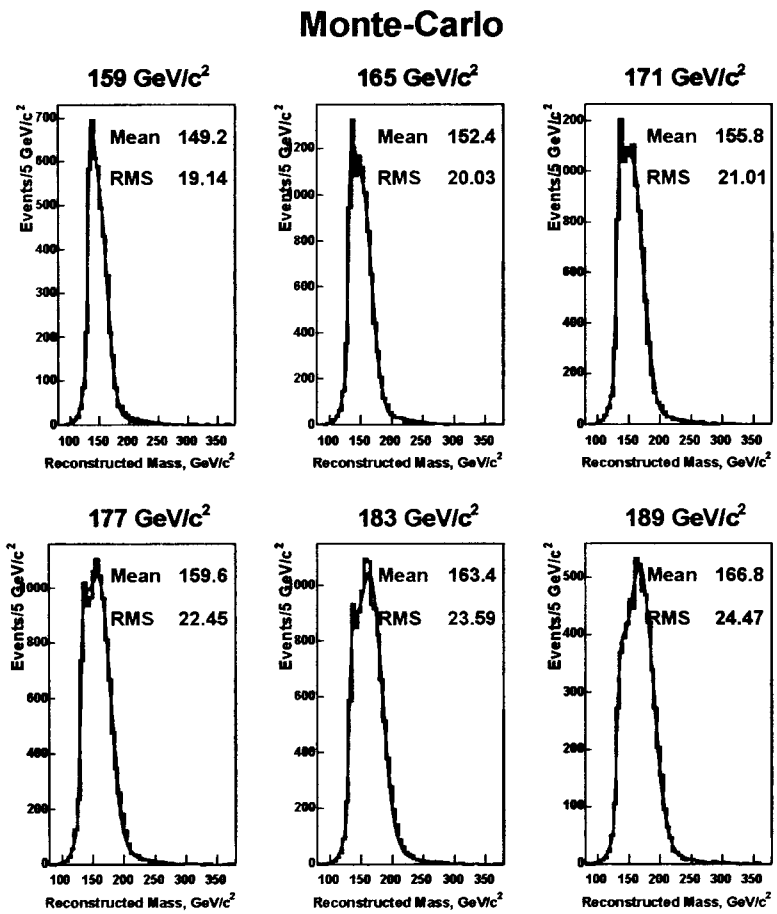

Figure 7: The examples of the signal templates

5.2 Background template

We used for background processes official Gen.6 MC samples ($WZ \to ll$, $WW \to ll$, $ZZ \to ll$, Drell-Yan, $Z \to \tau\tau$). Template for fake events was obtained by weighting the fakeable events from W+jets data sample according to the fake rate probability matrix [7]. In order to build general template for Drell-Yan events the templates for each sub-process were combined using their cross-sections and acceptances.

The obtained templates for these processes were combined together according to the expected number of events, as derived by the $t\bar{t}$ cross section group [7]; we show these numbers in Table (1).

Table (2) shows the main components of background and the samples we used to obtain background template.

	$n_j = 0$	$n_j = 1$	$n_j \geq 2$
WW	91.66±7.54	15.96±1.34	3.90±0.36
WZ	10.00±0.83	4.55±0.38	1.43±0.13
ZZ	2.41±0.04	0.65±0.02	0.34±0.02
$Z/\gamma^* \to ee$	72.43±15.79	25.93±6.05	7.75±2.24
$Z/\gamma^* \to \mu\mu$	18.88±5.32	8.88±2.74	3.40±1.15
$Z/\gamma^* \to \tau\tau$	35.54±3.24	26.46±2.47	7.31±0.89
Fakes	244.09±46.41	76.79±14.59	29.85±5.86
background	475.01±51.58	176.52±16.98	53.99±6.60
$t\bar{t}, \sigma = 6.7$ pb	1.18±0.06	17.29±0.56	60.53±1.88
Predicted	**476.19±31.58**	**176.52±16.98**	**114.51±7.00**
Observed	**443**	**187**	**129**

Table 1: Predicted and observed events in $1.1 fb^{-1}$, with details of the background contributions. The opposite charge requirement is applied.

The templates for different background components along with the combined background template are shown in Fig. 8.

The fitting function, f_b, is a slightly bit different from the one used for signal

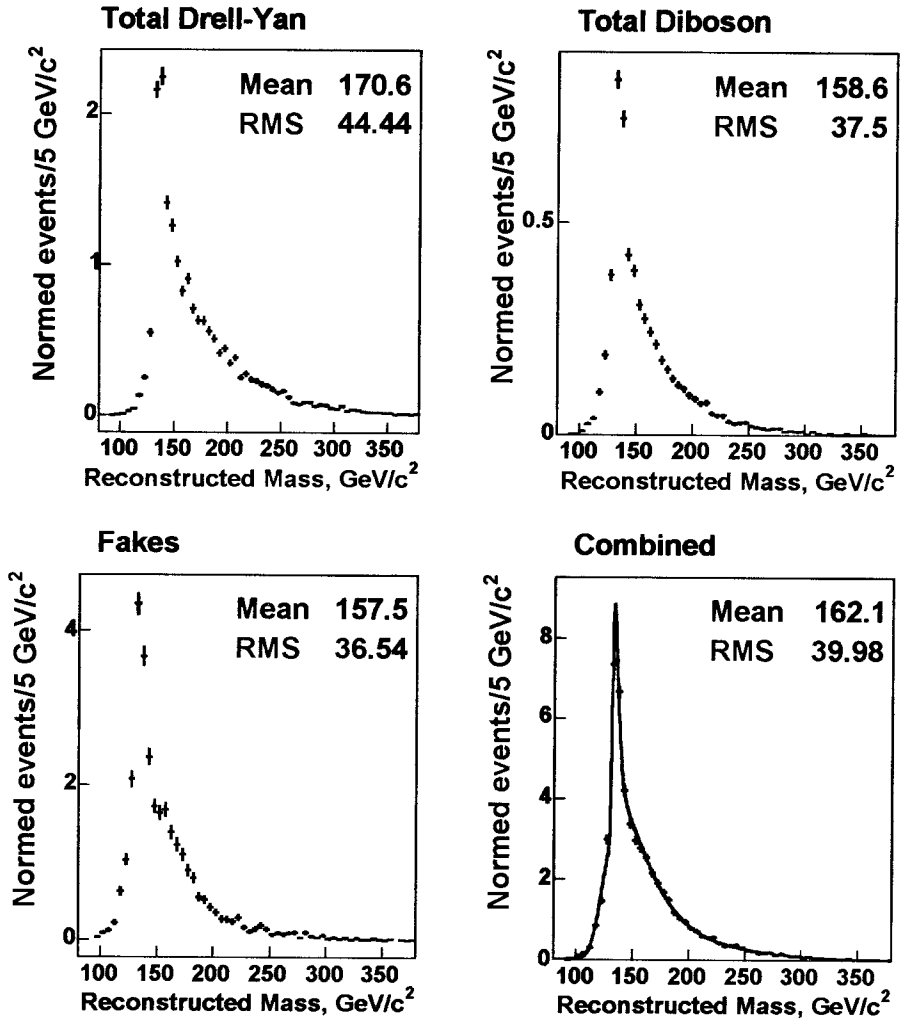

Figure 8: Templates of background processes Drell-Yan, Diboson, "fake" events. Lower right plot shows the combined background.

Background process	Samples
WW	itopww, wewkbd
WZ	itopwz, wewkcd
ZZ	itopzz
DY ee samples	ztop2p, ztopzb, ztop3p, xtop2p, xtoppb, xtop3p, ytop2p
DY $\mu\mu$ samples	ztop7p, ztopzt, ztop8p, xtop7p, xtoppc, xtop8p, ytop7p
DY $\tau\tau$ samples	ztopt2, xtopt2, zttt2h
Fakes	W+jets data

Table 2: Samples for background templates.

templates, as you can see from the formula (17).

$$f_b(M_t^{reco}) = q_7(q_6\frac{1}{\sqrt{2\pi}q_2}e^{-0.5(\frac{M_t^{reco}-q_1}{q_2}+e^{-\frac{M_t^{reco}-q_1}{q_2}})}+ \quad (17)$$
$$+(1-q_6)\frac{1}{\sqrt{2\pi}q_5}e^{-0.5(\frac{M_t^{reco}-q_4}{q_5})^2}) + (1-q_7)\frac{1}{\sqrt{2\pi}q_3}e^{-0.5(\frac{M_t^{reco}-q_8}{q_3}+e^{-\frac{M_t^{reco}-q_8}{q_3}})}$$

However, the main difference from f_s is: the f_b parameters $q_1, \ldots, q_8$ are not depend from the top mass:

$$q_k = \beta_k \quad (18)$$

6 Results from pseudo-experiments

We checked whether the fit with likelihood form (11) was able to return the correct mass by performing the "sanity check" pseudo-experiments for different input top mass values.

According to guidelines [10] the numbers of signal and background events in PE's were Poisson distributed with mean values as their expected numbers. We took as expected numbers 108.95±3.38 and 97.18±11.88 for signal and background respectively. These values were obtained using scaling from 1.1 to 2 fb^{-1}.

The output M_{top} (median of distribution) vs. input M_{top} is shown in (Fig. 9,left).

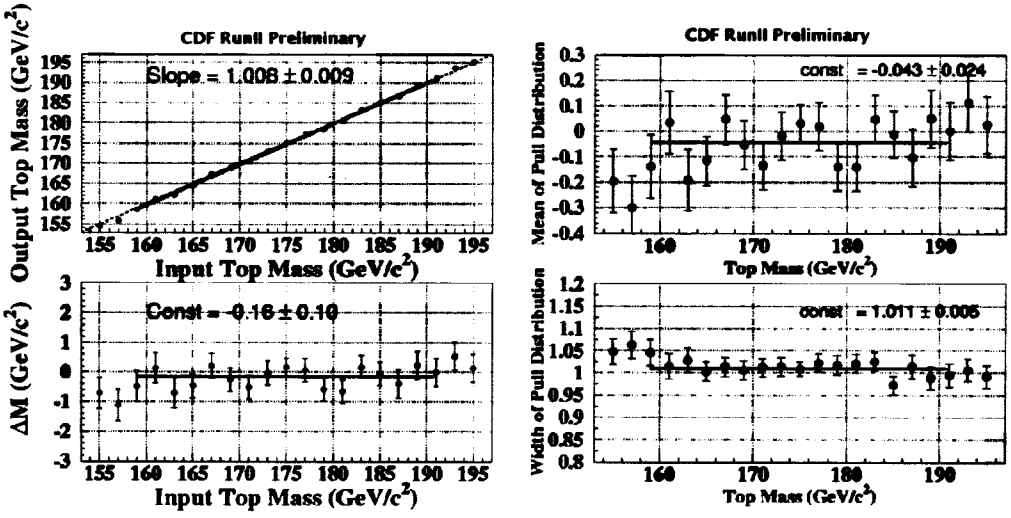

Figure 9: Left: The extracted top mass as a function of input mass. The result of a linear fit is also shown. The lower plot shows the residuals (reconstructed - input top mass). Right: Mean (above) and σ (below) of pull distributions determined from the pseudo-experiments as a function of input top mass.

A linear fit yielded a slope of 1.008±0.009. The mean and width of the pull distributions as a function of input top mass are shown in (Fig. 9,right).

The correction for the top mass mean value is 0.16±0.10 GeV/c^2. It is obtained from the fit of the distribution: residual vs. top mass (see Fig. 9,left).

The obtained correction for pull width is 1.011.

We checked the obtained corrections for top mass value and errors on the set of pseudo-experiments. The results are presented in Figure 10.

One can see now that the residual is equal to 0.0 (Fig. 10,left) and the width of pull distribution is 1.0 (Fig. 10,right) in the frame of errors.

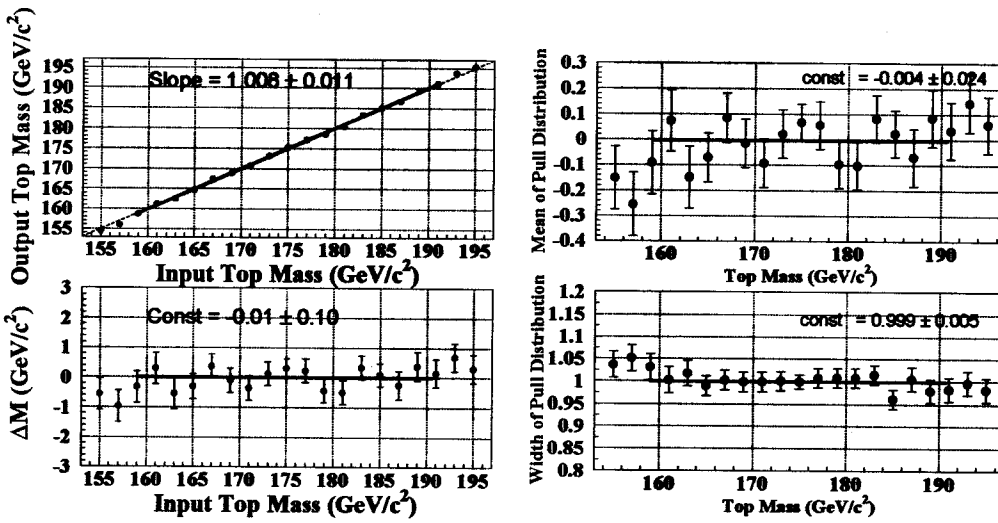

Figure 10: Left: The extracted top mass as a function of input mass after applying the corrections for mean value and for errors. The result of a linear fit is also shown. The lower plot shows the residuals (reconstructed - input top mass). Right: Mean (above) and σ (below) of pull distributions determined from the pseudo-experiments as a function of input top mass. Corrections for mean value and for errors are applied.

We estimated the expected statistical error of top quark mass measurement using an MC sample with top mass = $175 GeV/c^2$ (see Figure 11). The error is expected to be $4.3 GeV/c^2$ and taking into account the pull width correction finally we obtain $4.4 GeV/c^2$.

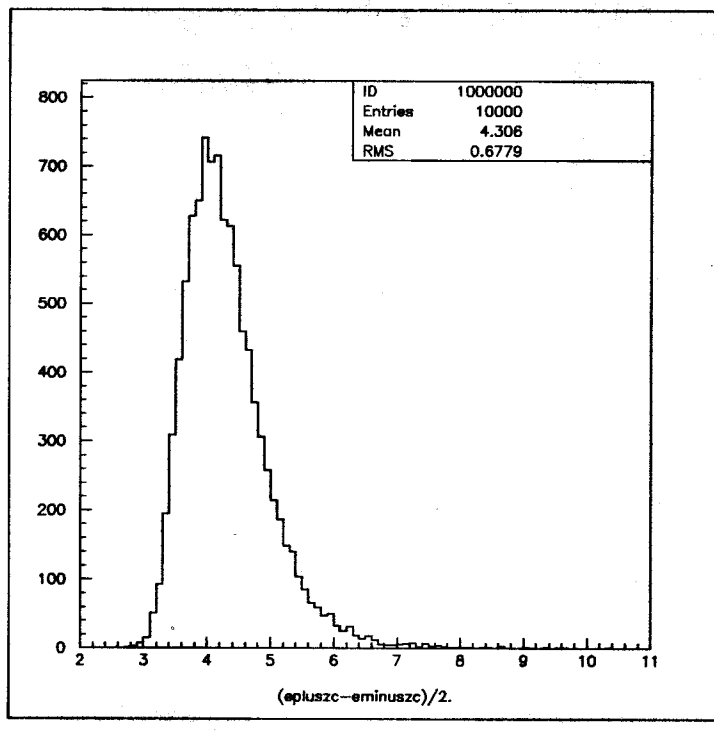

Figure 11: Statistical error distribution for top mass measurement @ MC sample with top mass= $175 GeV/c^2$

7 Blind test results

Before "opening the box" with data we performed test on the "blind" MC samples. The differences between extracted and true mass values for different "blind" samples in random order are shown in Table 3. The results are good: we have determined the top masses for blind samples with expected accuracy.

$M_{rec.}$ - M_{true} (GeV/c^2)	errors (GeV/c^2)	number of sigmas
0.6	1.2	0.5
-0.4	1.2	0.3
1.4	1.2	1.2
-0.9	1.2	0.8
0.3	1.2	0.2
1.4	1.2	1.1
0.3	1.2	0.3
0.0	1.2	0.0
-0.6	1.2	0.5
0.6	1.2	0.5

Table 3: Results on the blind samples

We present Figures concerning the "blind" samples here. These are the distributions of residuals, statistical errors and pull of pseudo-experiments for determination of the "blind top masses" (see Figure 12). The biases for the mean value (Figure 13,left) and the pull width (Figure 13,right) are also presented. We can stress that the bias in pull width conforms to the estimated one: 1.011 ± 0.005.

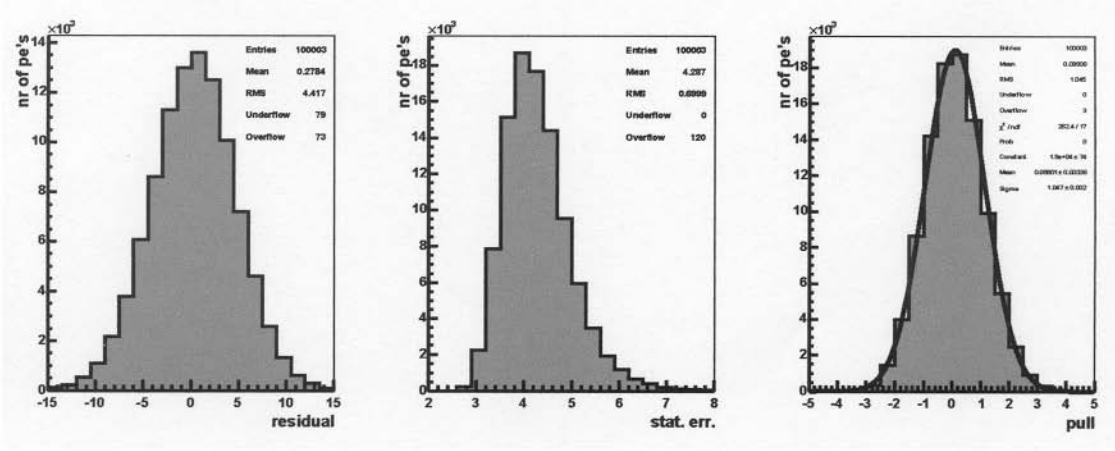

Figure 12: From left to right shown: residuals, statistical errors and pull distribution for pseudo-experiments for determination of the "blind" top masses

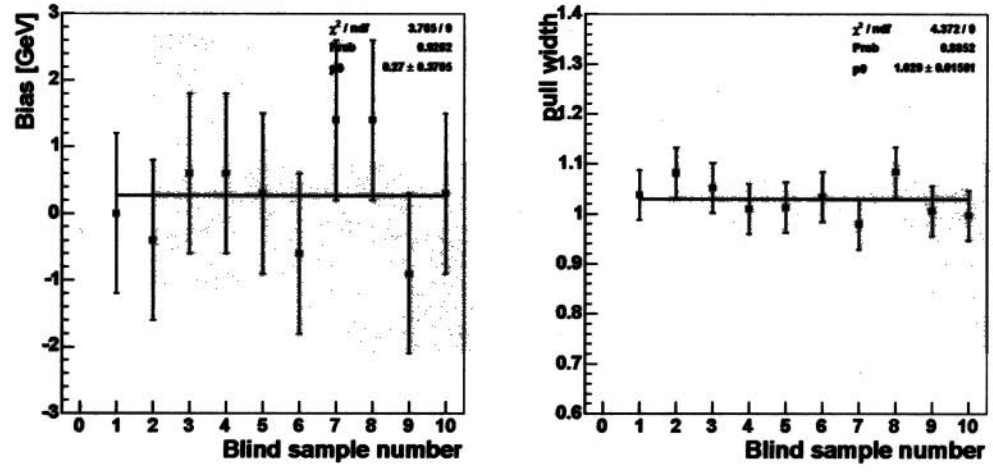

Figure 13: Left: The bias for the blind samples top masses. Right: The bias in the pull width for the blind samples.

8 Systematic Uncertainties

We have considered the following sources of systematic uncertainties on the fitted mass value: a) jet energy scale, b) amount of initial and final state radiation, c) shape of the background template, d) parton distribution functions, and e) approximations made by Monte Carlo generators, f) b-jet energy scale and lepton energy scale. The magnitudes of these uncertainties were estimated using large Monte Carlo samples generated only for the systematics study.

The procedure for estimating the systematic uncertainty is similar for all sources. For each source we varied the input value as appropriate (by 1σ, or changing PDF, etc) and evaluated the impact on the returned top mass. This was done by simulating a large number (usually 10000 or more) of pseudo-experiments (PE) with the nominal assumption and with the alternate assumption. The reconstructed mass distribution from each PE was fitted with the same likelihood procedure. The obtained mass value was entered into an ensemble of results of simulated experiments. The systematic uncertainty assigned to our measurement is the difference in the average of these result distributions for the nominal and shifted ensembles or half the difference between results obtained with $+\sigma$ and $-\sigma$ of the corresponding parameter change.

8.1 Jet Energy Scale

In Run 2 the jet systematic uncertainty is included in the jet correction software package. It is possible to turn on a $\pm$ 1σ change in the energy scale for the specific type of jet correction. A detailed description of each source of uncertainty can be found at Jet Energy and Resolution Group Web Page [11].

By means of the above-described PE we estimated the mass shift caused by different corrections. We obtained the overall uncertainty of 2.9 ± 0.03 GeV/c^2 shifting jets in both signal and background MC events by $\pm\sigma$ of the total jet energy systematic uncertainty.

Individual contributions to the systematic uncertainty are presented in Table 4.

8.2 Radiation effects, generators and B-jet energy scale

The effects of initial (ISR) and final (FSR) state radiation on the returned top mass were studied using Pythia as a signal generator. To estimate the uncertainty

Level	Source	M_{rec} (GeV/c^2)		Uncertainty (GeV/c^2)
		$+\sigma$	$-\sigma$	$\Delta M_{rec}/2$
1	η-dependent	175.80	174.58	0.61 $\pm$0.03
4	multiple interactions	175.20	175.16	0.02 $\pm$0.03
5	absolute scale	177.26	172.93	2.17 $\pm$0.03
6	underlying event	175.37	175.05	0.16 $\pm$0.03
7	out-of-cone	176.99	173.36	1.81 $\pm$0.03
8	splash-out	175.49	174.94	0.28 $\pm$0.03
total	sum in quadrature			2.91 $\pm$0.07
100	alltogether sources	177.95	172.17	2.88 $\pm$0.03
total				**2.9**

Table 4: Mass shifts indicated by the PE when the jet energy is shifted by $\pm 1\sigma$ of each separate correction.

induced by ISR we studied the difference between ISR enhanced and reduced samples, as recommended by the top group. The half-difference between average reconstructed top masses from these samples is assigned as a systematic uncertainty from ISR. To estimate the uncertainty induced by FSR we used the Pythia with enhanced and with reduced amount of FSR.

The results for the ISR and FSR induced systematic are summarized in Table 5.

The effect of using different top Monte Carlo generators was checked by comparing nominal Pythia with Herwig samples. The obtained mass shifts are presented in Table 5.

Source		Datasets	Mass GeV/c^2	Mass Shift GeV/c^2	Syst. GeV/c^2
B-JES	$\pm$ 1% shift in JES for b-jets	ttkt75(-)	174.15$\pm$0.04	$\Delta M/2$ =1.04$\pm$0.03	0.62
		ttkt75(+)	176.24$\pm$0.04		
Gener.	Herwig	htop75	174.71$\pm$0.32	ΔM =0.46$\pm$0.35	0.46
	Pythia	ttkt75	175.17$\pm$0.15		
ISR	More ISR	itoprk	175.00$\pm$0.32	ΔM =-0.17$\pm$0.34	0.34
	Less ISR	itoprl	174.95$\pm$0.32	ΔM =-0.22$\pm$0.34	
FSR	More FSR	ftoprj	175.05$\pm$0.32	$\Delta M/2$ =0.17$\pm$0.22	0.22
	Less FSR	ftoprl	175.38$\pm$0.32		

Table 5: Top mass shifts obtained from the PE for different Monte Carlo samples.

8.3 Background Shape

Background composition.

In order to estimate effect on top mass from the uncertainty in background composition we varied the contribution in combined background template of main sources (Diboson, Drell-Yan and "fakes") by $\pm\sigma$. Contribution from another subsamples was corrected to maintain the total expected number of background events. As result 6 alternative combined background templates were obtained and used for

PE's. Obtained top mass shifts presented in Table 6. We assigned 0.46 GeV/c^2 as

Source		Mass GeV/c^2	Mass Shift GeV/c^2	Syst. GeV/c^2
BG compos-	Diboson($-\sigma$)	175.15±0.04	$\Delta M/2$ =-0.02±0.03	0.03
ition	Diboson($+\sigma$)	175.11±0.04		
	DY($-\sigma$)	174.90±0.04	$\Delta M/2$ =0.25±0.03	0.25
	DY($+\sigma$)	175.40±0.04		
	Fakes($-\sigma$)	175.53±0.04	$\Delta M/2$ =-0.39±0.03	0.39
	Fakes($+\sigma$)	174.74±0.04		
				0.46
Fake	-linear E_T-dependent shift	174.80±0.04		
shape	in fake rate matrix		$\Delta M/2$ =0.41±0.03	0.41
	+linear E_T-dependent shift	175.61±0.04		
	in fake matrix			
Drell-Yan	decreased weight	174.88±0.04		
shape	in the Z window		$\Delta M/2$ =0.30±0.03	0.30
	increased weight	175.48±0.04		
	in the Z window			

Table 6: Top mass shifts obtained from the PE for different BG composition and fake shape.

our systematic error for composition in combined background template.

"Fake" events template shape.

In order to study how the uncertainty for "fake" events template shape can affect our resulting top mass we inserted linear E_T-dependent shift for values in our fake rate matrix. New fake rates were calculated according to the formula:

$w_{\pm} = w_0 \pm 1/8 \times (2 \times i_{E_T} - 8) \times \sigma_w$

were w_0 is the unshifted fake rate, σ_w is the uncertainty on w_0, and i_{E_T} denotes

the E_T bin. Two new fake templates were obtained using changed fake rate matrix and included in combined background template. Using these templates for PE's we got shifts in top mass as presented in Table 6. We took 0.41 GeV/c^2 as our systematic error for uncertainty in template for "fake" events shape.

Drell-Yan template shape.

In order to suppress Drell-Yan events($Z/\gamma^* \rightarrow ee, Z/\gamma^* \rightarrow \mu\mu$) we have the increased requirement on missing E_T for events with effective mass of lepton and track lepton inside Z-window (Z-veto cut). Drell-Yan events can get significant value of missing E_T only because mismeasurement of jets E_T. Differencies between modeling of this effect and the reality can give us the shifted top mass. In order to estimate the sensitivity of our measurement to this we increased (and decreased) by factor of 2 the weight in $Z/\gamma^* \rightarrow ee, Z/\gamma^* \rightarrow \mu\mu$ templates for events which have effective mass of lepton and track lepton inside Z-window. Two new combined background templates were obtained using this changed $Z/\gamma^* \rightarrow ee, Z/\gamma^* \rightarrow \mu\mu$ templates. Then we got from PE's the shifts in the top mass as presented in Table 6. We took 0.3 GeV/c^2 as our systematic error due to uncertainty in Drell-Yan template shape.

8.4 Parton Distribution Functions

The uncertainty induced by PDF's was assessed by comparing CTEQ5L vs MRST in Pythia. The results are listed in Table 7. The recently developed next-to-

Source	Mass Shift GeV/c^2	Syst. GeV/c^2
CTEQ PDFs	Sum($\Delta M/2$)=0.21±0.13	0.21
CTEQ5L vs MRST72	ΔM=0.07±0.06	0.07
α_s (MRST72 vs MRST75)	ΔM=-0.22±0.06	0.22
Total		0.31

Table 7: PDF Systematic

leading order PDF from CTEQ6 [12] allows us to vary some PDF sets within their uncertainty. The possible variations are separated into contributions from 20

independent eigenvectors, so in total we have 41 different sets (1 nominal and 2×20 for $\pm 1\sigma$ variations). The PDF effect is studied using the reweighting method [13], where reconstructed top mass templates for each PDF set are obtained from one single sample (Pythia 175 GeV/c^2 sample) by weighting the mass for each event by the probablity for that event to proceed according to the given PDF. Results for the nominal PDF and for the 20 pairs of $\pm 1\sigma$ PDFs are shown in Fig. 14. The black line corresponds to the nominal PDF set. The total PDF uncertainty was

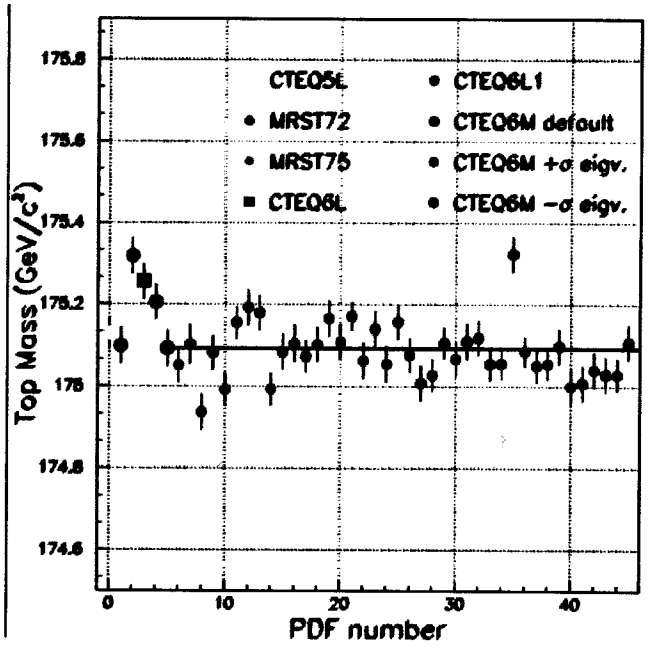

Figure 14: Results used for PDF uncertainty

estimated as 0.31 GeV/c^2.

8.5 Lepton energy scale

The effect on the top mass from the uncertanty on lepton energy scale was studied by applying $\pm 1\%$ shifts for lepton p_T [14]. Resulting top masses are 175.48 GeV/c^2 and 174.84 GeV/c^2. We take the half difference (0.3 GeV/c^2) as our systematic error from lepton energy scale uncertainty (see Table 8).

8.6 Summary of Systematic Errors

The summary of systematic uncertainties are listed in Table 8. For each source of systematic uncertainty we choose the obtained from PE mass shift or its error, which one is bigger.

CDF RunII Preliminary

Source	Uncertainty (GeV/c^2)
Jet Energy Scale	2.9
b-JES	0.6
Initial State Radiation	0.3
Final State Radiation	0.2
Parton Distribution Functions	0.3
Monte-Carlo Generators	0.5
Background composition	0.5
Fakes shape	0.4
DY shape	0.3
Lepton energy scale	0.3
Total	**3.1**

Table 8: Symmary of systematic uncertainties

9 Data

The data sample we used in our analysis includes data collected between March 2002 and May 2007 and corresponds to a total integrated luminosity of 2.1 fb^{-1}.

We selected 236 top event candidates. The background was rescaled from track+lepton cross section measurement (1.1 fb^{-1},[7]) and the estimated value is N_b=105.8±12.9.

The two-component, background-constrained fit (N_b=105.8±12.9) for the obtained l+trk sample returns: $M_{top} = 167.57 \pm^{4.15}_{3.99}$ GeV/c^2, with $126.13\pm^{17.99}_{17.41}$ signal events and $108.3\pm^{11.6}_{11.5}$ background events.

The fitted mass distribution is shown in Fig. 15. The insert shows the mass dependence of the negative log-likelihood function.

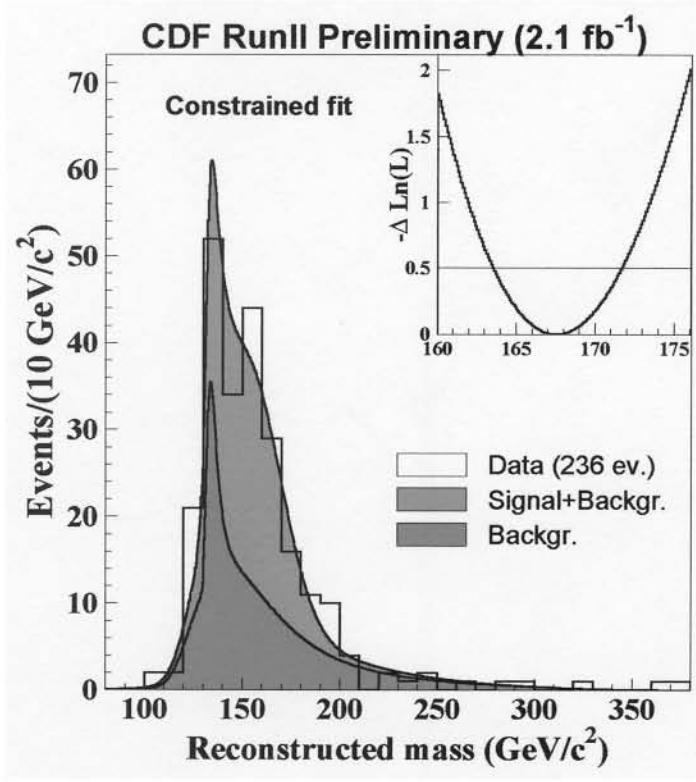

Figure 15: Two-component, constrained fit to the l+trk sample. The pink solid area corresponds to the background returned by the fit and the blue area is the sum of background and signal events. The insert shows the mass-dependent negative log-likelihood used in the fit.

We also performed a fit when the number of the background events was unconstrained, see Fig. 16. This fit returns $M_{top} = 167.59\pm^{4.42}_{4.21}$ GeV/c^2, with $117.82\pm^{26.48}_{26.59}$

signal events and $118.18 \pm^{27.53}_{25.52}$ background events.

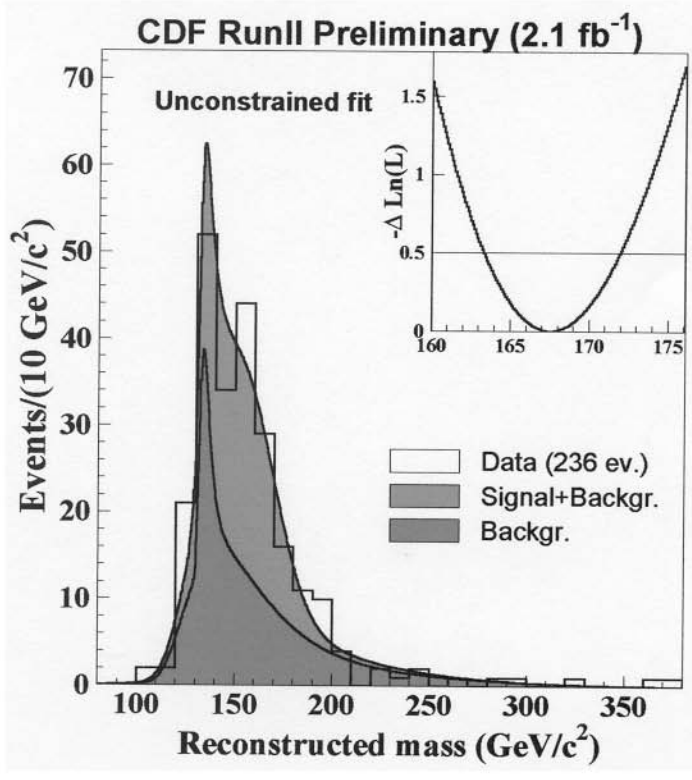

Figure 16: Two-component, unconstrained fit to the l+trk sample. The pink solid area corresponds to the background returned by the fit and the blue area is the sum of background and signal events. The insert shows the mass-dependent negative log-likelihood used in the fit.

Expected statistical errors obtained from the pseudo-experiments are shown on Fig 17. The plot shows the stat. error distribution for the top mass of 167 GeV/c^2. The arrows indicate the errors returned by the fit to the data. The probability to have better accuracy than our one from data is 83%.

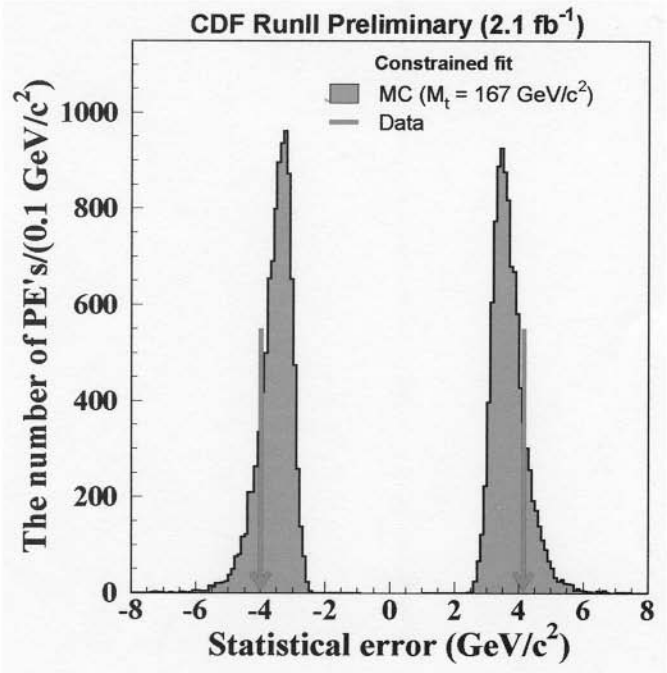

Figure 17: Expected statistical errors for different top masses. The arrows indicate the errors returned by the fit to the data.

10 Conclusion

We applied the neutrino ϕ weighting method to solve a non-constrained kinematics of the top quark decay in dilepton mode.

236 candidate events were selected from the data sample with integrated luminosity of 2.1 fb^{-1}. Our preliminary measurement of the top quark mass in the l+trk sample is: $M_{top} = 167.7 \pm^{4.2}_{4.0}$ (stat) $\pm$ 3.1 (syst) GeV/c^2. Statistical errors are shown here after multiplying by factor of 1.011 and the mean value increased on 0.16 GeV/c^2 - the values obtained from our pseudo-experiments.

Appendix

In this appendix we show the kinematical distributions which have been obtained to validate our data sample for CDF integrated luminosity 2.1 fb^{-1}. The distributions for $N_{jet} \geq 2$ events were obtained on the data sample selected for our top mass measurement. The distributions for $N_{jet} = 0$ and $N_{jet} = 1$ events were obtained on the data sample with relaxed cuts on the number of jets per event.

The plot 18 shows the comparison between observed and predicted numbers of events. The number of predicted events for the plots (19-24) is scaled to be equal to the number of observed ones. The relative backgrounds and signal contribution for predicted events is done according to the x-section group measurements [7].

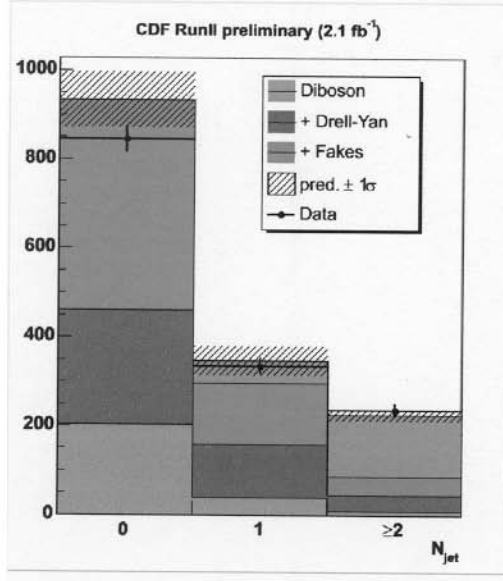

Figure 18: Number of predicted events compared to the number observed in the data. The shaded areas show the (1σ) uncertainties on the predicted numbers.

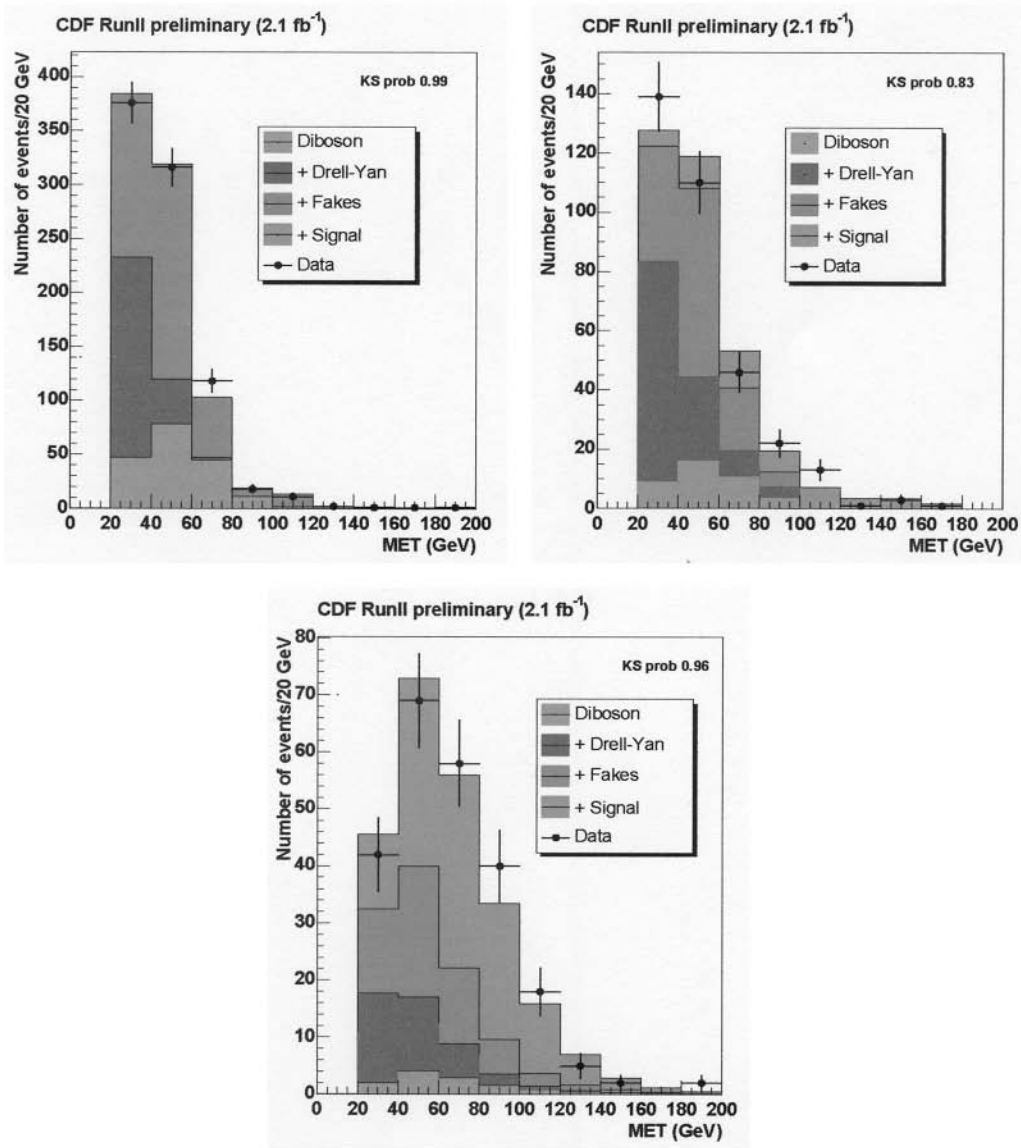

Figure 19: Missing E_t distribution of predicted and candidate events. The plots are for different number of jets in the events. Top left: $N_{jet} = 0$, top right: $N_{jet} = 1$, bottom: $N_{jet} \geq 2$

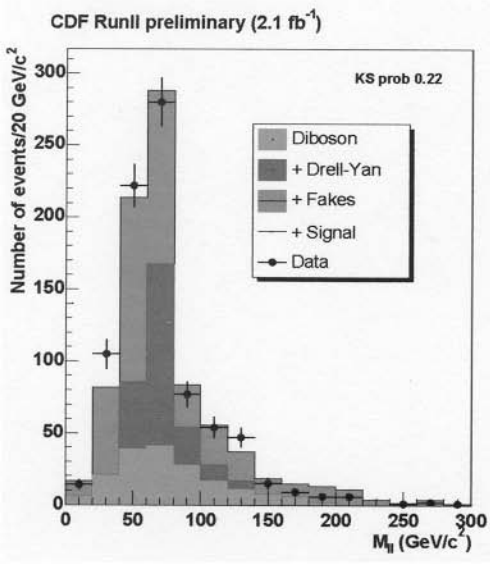

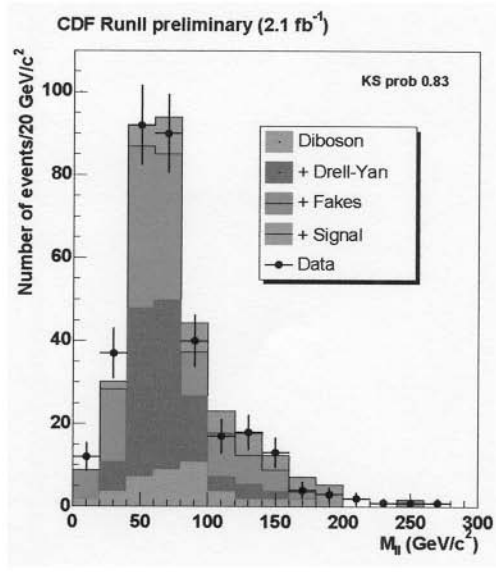

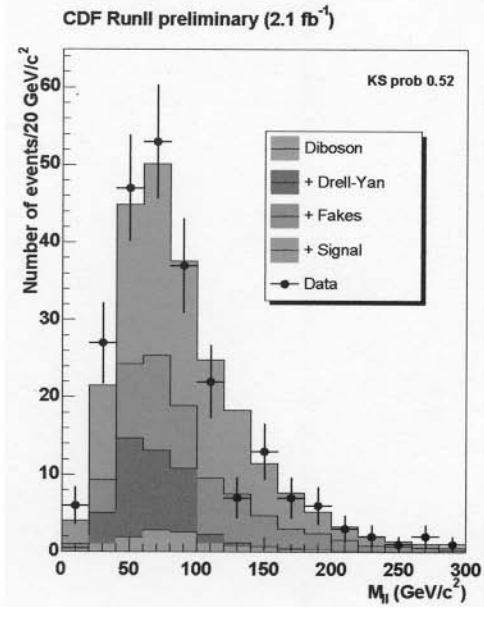

Figure 20: Invariant mass of the tight lepton - track lepton pair in predicted and candidate events.The plots are for different number of jets in the events. Top left: $N_{jet} = 0$, top right: $N_{jet} = 1$, bottom: $N_{jet} \geq 2$

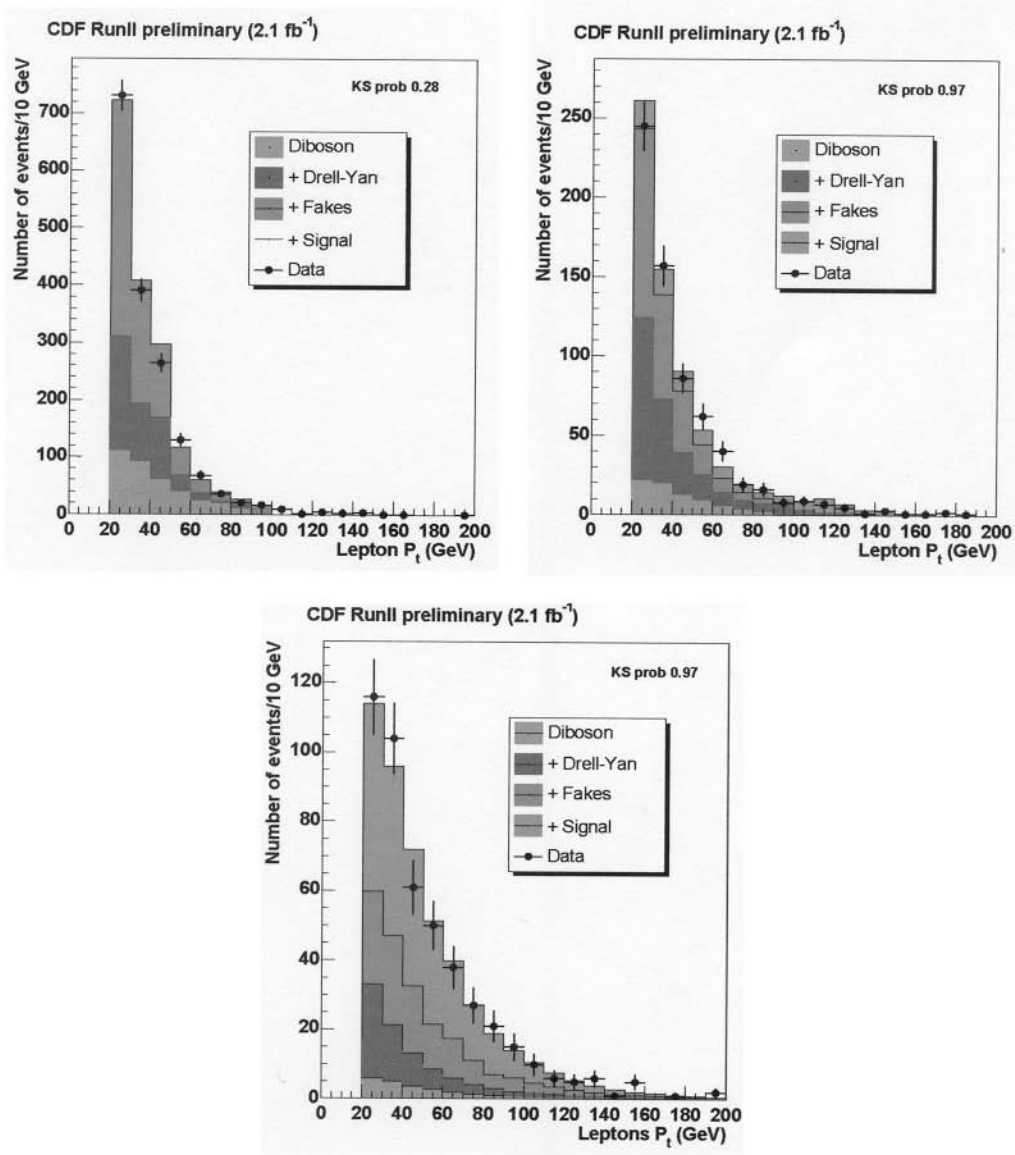

Figure 21: Transverse momentum of both lepton candidates in predicted and candidate events.The plots are for different number of jets in the events. Top left: $N_{jet} = 0$, top right: $N_{jet} = 1$, bottom: $N_{jet} \geq 2$

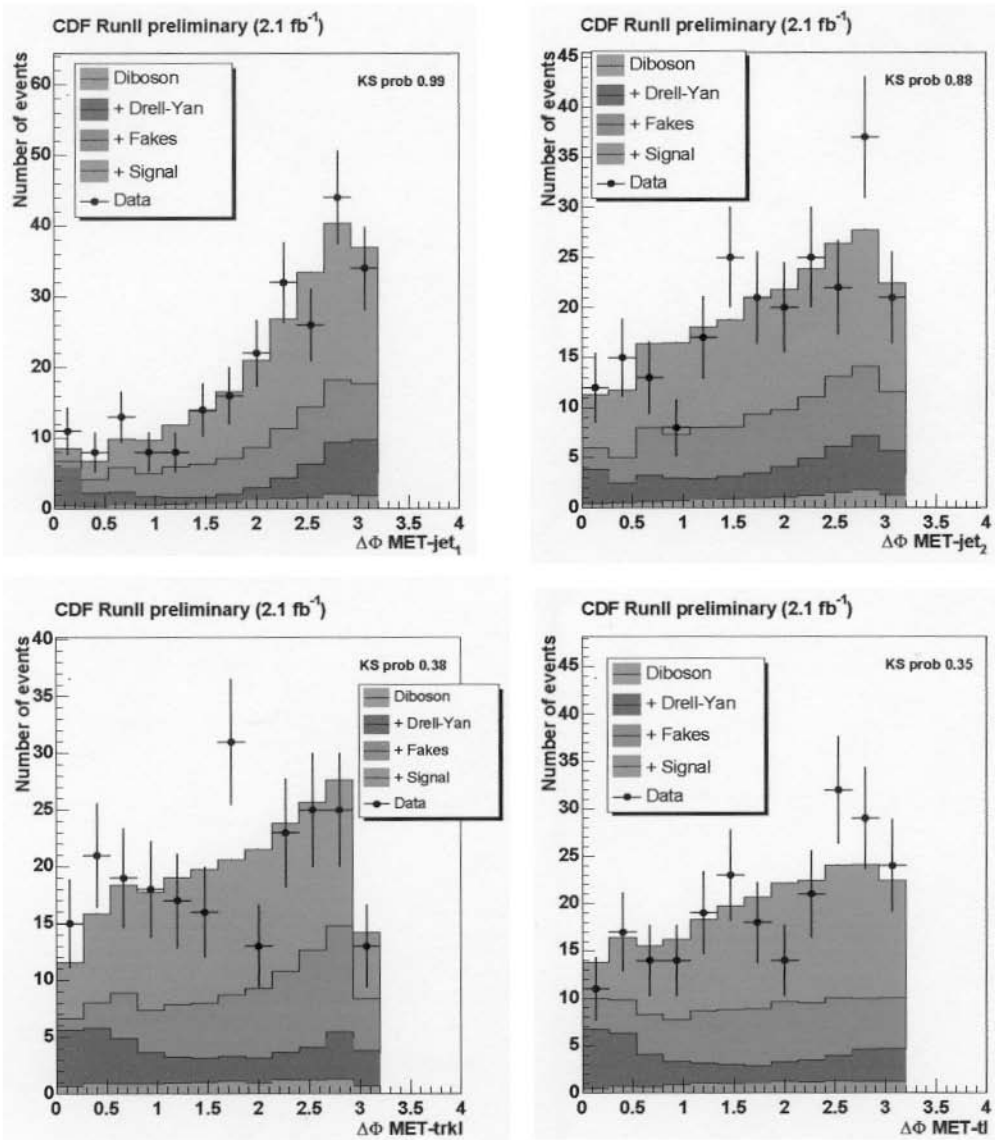

Figure 22: These distributions are for number of jets in the events $N_{jet} \geq 2$. Upper left plot: $\Delta\phi$ between missing E_t and leading E_t jet. Upper right plot: $\Delta\phi$ between missing E_t and second leading E_t jet. Bottom left plot: $\Delta\phi$ between missing E_t and isolated track. Bottom right plot: $\Delta\phi$ between missing E_t and tight lepton.

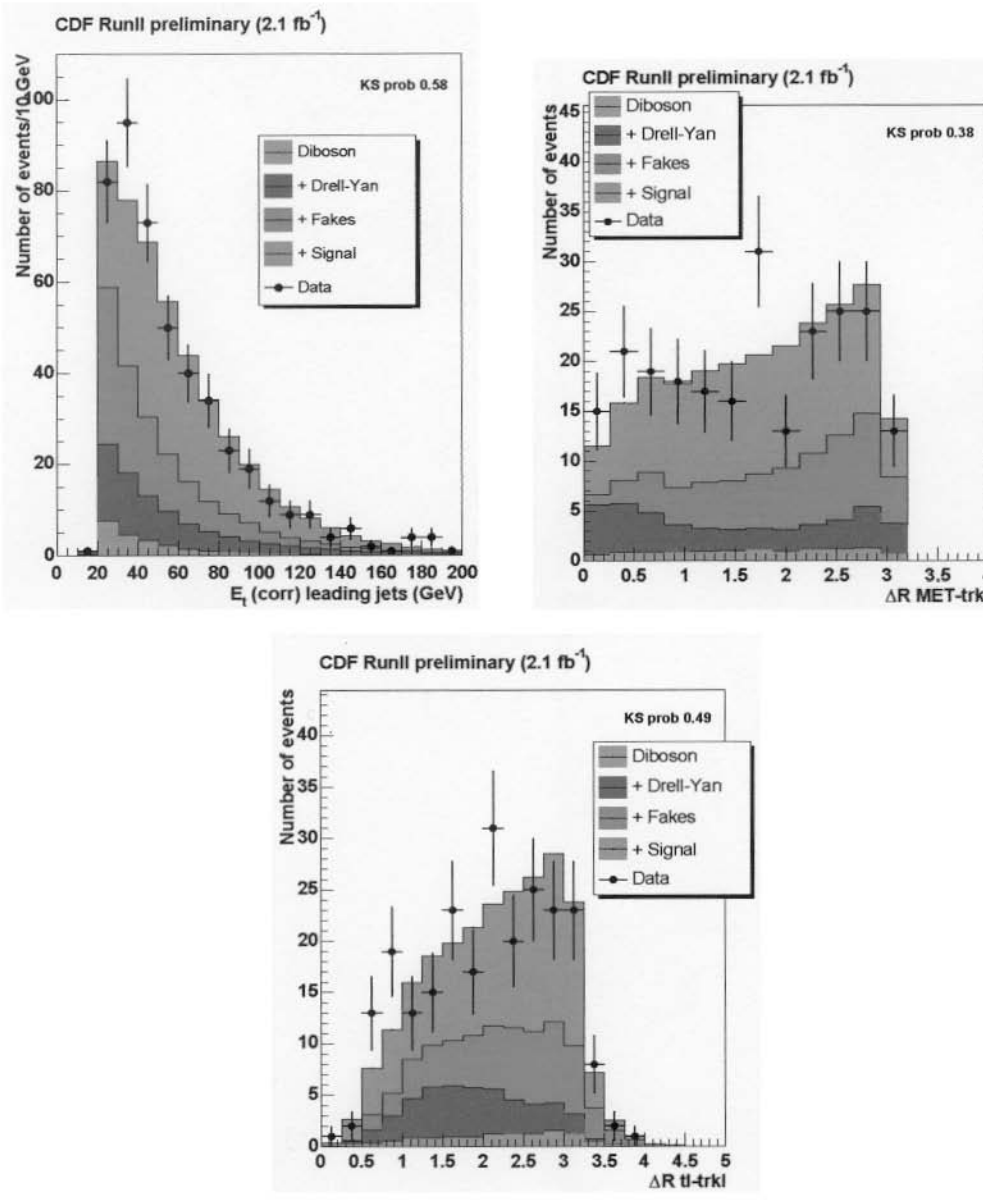

Figure 23: These distributions are for number of jets in the events $N_{jet} \geq 2$. Upper left plot: E_t distribution of the leading jet. Upper right plot: ΔR between missing E_t and isolated track. Bottom plot: ΔR between tight lepton and isolated track.

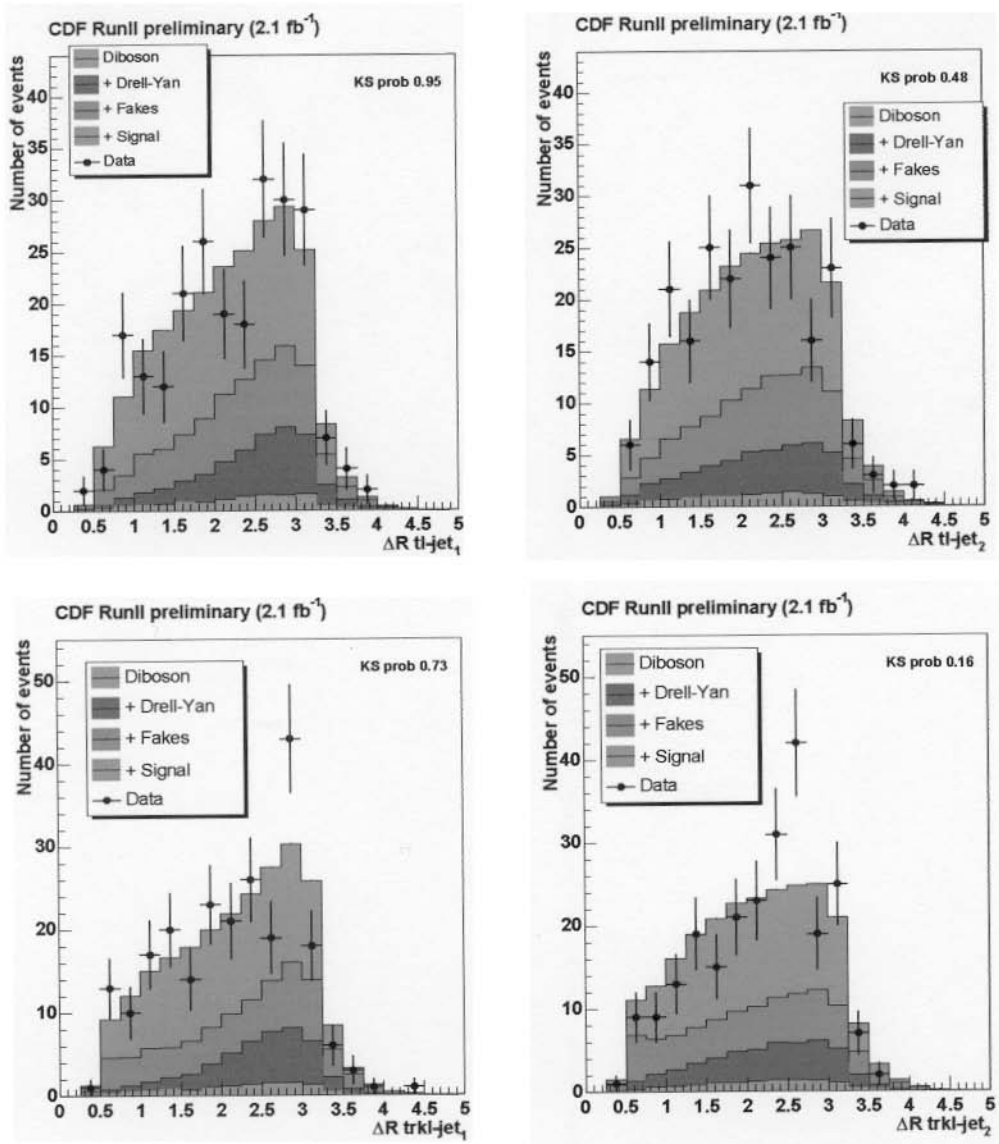

Figure 24: These distributions are for number of jets in the events $N_{jet} \geq 2$. Upper left plot: ΔR between tight lepton and and leading E_t jet. Upper right plot: ΔR between tight lepton and second leading E_t jet. Bottom left plot: ΔR between isolated track and leading E_t jet. Bottom right plot: ΔR between isolated track and second leading E_t jet.

References

[1] G. Bellettini, J. Budagov, G. Chlachidze, V. Glagolev, F. Prakoshyn, A. Sissakian, I. Suslov, G. Velev. Summer 2004 Top Mass Measurement in Dilepton Events using the MINUIT Fitter *CDF Internal Note 7093*, 2004

[2] G. Bellettini, J. Budagov, G. Chlachidze, V. Glagolev, F. Prakoshyn, A. Sissakian, I. Suslov, G. Velev. Top Mass Measurement in Dilepton Events using Neutrino ϕ Weighting Method. *CDF Internal Note 7641*, 2005

[3] CDF Collaboration, Measurement of the Top Quark Mass using Template Methods on Dilepton Events in Proton-Antiproton Collisions at sqrt(s)=1.96 TeV. *Phys.Rev. D73 (2006) 112006* ,2006.

[4] D. Acosta *et al.* Phys. Rev. D71, 032001 (2005). The CDFII Detector Technical Design Report, Fermilab Report No. Fermilab-Pub-96/390-E.

[5] W.-M. Yao et al., 2006 Review of Particle Physics *J. Phys. G 33, 1 (2006)*

[6] Giorgio Bellettini, Julian Budagov, Guram Chlachidze, Vladimir Glagolev, Fiodar Prakoshyn, Alexei Sissakian, Igor Suslov, George Velev. Measurement of the Top Quark Mass using the Minuit Fitter in Dilepton Events at CDF. *CDF Internal Note 7239*, 2004

[7] J. Thom, J. Incandela, C. Mills, P. Savard, T. Spreitzer. A Measurement of the Top Dilepton Cross-Section using the 1.1 fb^{-1} Tight Lepton and Isolated Track Sample. *CDF Internal Note 8696*, 2007

[8] http://www-cdf.fnal.gov/internal/dqm/goodrun/v17/DQM Beamlines.html

[9] T. Maki, J. Antos, A. Beretvas, Y.C. Chen, R. Lysak. Cross-section Dependent Top Mass Measurement in Dileptonic Channel using Template Method. *CDF Internal Note 8823*, 2007

[10] http://www-cdf.fnal.gov/internal/physics/top/run2mass/guidelines.html

[11] Jet Energy and Resolution Group Web Page at http://www-cdf.fnal.gov/internal/physics/top/jets/corrections.html

[12] J.Pumplin et al., "New generation of parton distributions with their uncertainties with global QCD analysis",hep-ph/0201195

[13] Stephen Miller, http://cdfrh0.grid.umich.edu/ miller/pdf/pdf_acceptance.html, 2004

[14] http://www-cdf.fnal.gov/internal/physics/top/run2mass/sys6.html